A Theory for Accelerated Stress Corrosion Cracking in Arc-Welded Aluminum Alloys and Mitigation by Precision Additive Dressing

T.E. Borchers, A. Seid, and W. Zhang

1. Introduction

To avoid hot cracking when welding a Cu-lean, high-strength 7xxx series (Al-Zn-Mg) aluminum alloy (AA), and maintain acceptable joint strength, 5xxx series (Al-Mg) filler wires are utilized [1] [2]. However, such welded joints have shown a tendency to develop stress corrosion cracking (SCC) [3] [4] [5] [6]. SCC of these joints has typically occurred within the heat-affected zone (HAZ) directly adjacent to the fusion line (FL) [7] [8]; the thermo-mechanically affected zone (TMAZ) in solid-state joints of Al-Zn-Mg alloys, created by friction-stir welding (FSW), has also shown susceptibility to SCC. However, the HAZ of fusion welds have proven more susceptible to SCC than the TMAZ of FSW [6] [9].

Anodic dissolution [10] [11] [12] [13] and hydrogen embrittlement (HE) [14] [15] [16] [17] are two largely debated mechanisms that describe SCC; both mechanisms possess substantial evidence, and likely contribute to SCC of Al-Zn-Mg alloys. Though the SCC mechanism is debated, it's generally agreed that three factors are necessary for SCC occurrence: (i) a corrosive environment, (ii) some threshold stress intensity, and (iii) a susceptible material. A study [18] claimed that anodic dissolution of precipitates causes pitting corrosion which promotes localization of plasticity (stress intensity), and induces local hydrogen discharge, entry and embrittlement around the pit. A further study [19] explains that within a pit, the local solution becomes more acidic (lower pH); acidic environments increase the corrosion rate of AAs [20].

The HAZ or TMAZ thermal cycles are such that a region, immediately adjacent to the fusion line, extending to some distance (depending on heat input) from the fusion line, experiences a temperature above the solvus of the strengthening precipitates for some length of time. Within the HAZ, strengthening precipitates for Al-Zn-Mg alloys (e.g. AA 7003 and AA 7005), η phase ($MgZn_2$), would dissolve [21], and as a consequence the HAZ would possess excess Zn and Mg in solid-solution. A study [22] shows that an increase of 3 wt% Zn in solid solution substantially decreases the metal's breakdown (pitting) potential (V_B); this supports why a lower V_B was noted in both a HAZ [23] and TMAZ [24]. Galvanic corrosion and preferential metallic dissolution (pitting) within the HAZ/TMAZ is induced because of lower potentials with respect to the base metal (BM) or fusion zone (FZ) [23].

Additionally, Cu-lean Al-Zn-Mg alloys naturally age, thus the HAZ will, shortly after welding, possess under-aged precipitation in the HAZ [25]; under-aged (T4) and peak-aged (T6) microstructures have proven more susceptible to SCC than over-aged (T7) microstructures [26]. Studies [27] [28] have claimed that a retrogression and re-aging (RRA) thermal cycle provides improvement of corrosion resistance over T6; however, others claim that Cu-lean alloys benefit less from the RRA heat treatment [29] [30]. It is noted that a typical automotive paint bake (PB) thermal cycle is very similar to a retrogression heat treatment without any re-aging; however, after the PB, natural aging will occur.

Furthermore, the HAZ possesses an equiaxed grain structure [23] [31] [25]. Equiaxed grains, like the short transverse direction, exhibit poor SCC resistance [13] [32]. Both the HAZ and TMAZ thermal cycles will dissolve η phase [21]. Thus, the summation of evidence suggests that whether an under-aged, equiaxed microstructure, susceptible to pitting and galvanic corrosion,

was created by solid-state or fusion welding, it should have a reasonably similar SCC response. This study attempts to explain why SCC is accelerated in fusion welds.

The authors' prior studies [5] [6] suggest that the precipitation of Cu-lean, electrochemically anodic, T phase [$(Al,Zn)_{49}Mg_{32}$] in the weld toe contributes to accelerated SCC failures of fusion welded AA 7003. The specific region of the weld toe that is enriched with T phase is termed a fused-overlap zone (FOZ); the FOZ typically extends 1 mm beyond the weld toe atop the weld heat-affected zone (HAZ).

This study investigates the relative SCC contribution of FOZ T phase, HAZ precipitation, and specimen strain of fusion welded AA 7003; the fracture surface analyzed in [5] revealed that the investigated failure was SCC. Also, herein, the feasibility of different engineering solutions for SCC of these weldments is compared.

2. Experimental Methods

The BM and filler metal for the welded specimens were AA 7003 and AA 5356 respectively. Each specimen was welded on the same robotic welding equipment with consistent weld parameters; the welding details are outlined within prior work [6]. Each subsequent processing step was performed on the welded lap-joint.

Some of the lap-joints underwent a milling procedure to remove the FOZ. The intention of milling was to eliminate the presence of FOZ T phase precipitation without altering other variables. Prior work [33] showed a possible reduction in HAZ strain due to geometric changes induced by post-weld milling. The depth of milling was decreased in an attempt to eliminate the reduction in HAZ strain.

Milling of the FOZ was conducted using a ball-nose end mill with a diameter of 6.35 mm (0.25 in.) perpendicular to the horizontal. The center of the end mill was aligned with the lower FOZ and traversed the entire longitudinal length of weld. A schematic of the milling setup is shown in Figure 1.

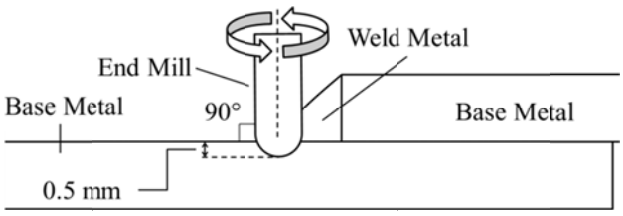

Figure 1: A schematic of post-weld milling of the FOZ using a ball-nose end mill

Other lap-joints underwent an EDM notching procedure; the intention was to increase the local stress intensity experienced within the specimens' HAZ, directly adjacent to the fusion line (interface between HAZ and FZ). The intent was to investigate whether FOZ T phase contributes towards stress intensity or the material's SCC susceptibility.

The EDM notching procedure used a wire EDM that possesses a cut diameter of 0.3 mm. On the BM, a distance 0.5 mm from the weld toe (WT), the EDM wire was held parallel to the WT. A schematic of this operation is shown in Figure 2. EDM Cut 1 was made at a vertical depth of 0.1 mm into the BM; this depth was maintained as the wire traversed towards the WT and beyond for a total distance of 1 mm. The idea of EDM Cut 1 was to remove the FOZ region that doesn't penetrate into the BM (i.e. removes T phase precipitation). The endpoint of EDM Cut 1 was the starting point for EDM Cut 2. EDM Cut 2 was made at a 45° angle with the horizontal for a length of 1 mm. The purpose of EDM Cut 2 was to increase the stress intensity experienced within the HAZ.

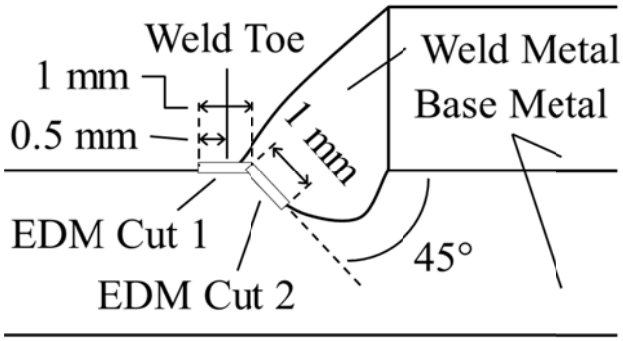

Figure 2: A schematic of the EDM notching procedure

Some specimens were exposed to a thermal cycle that simulates the heat exposure a joint would experience during a "paint baking" procedure. To simulate a paint bake thermal cycle (PBTC), specimens experienced 180°C for 30 minutes within an argon atmosphere and were immediately water-quenched upon removal from the furnace. The similarity of the PBTC to a retrogression thermal cycle is noted; according to Wu and Wang [27] the strengthening precipitates will have been altered by the PBTC to increase corrosion resistance. No painting is conducted on any specimen. Some as-welded specimens and EDM notched specimens were selected to experience the PBTC.

Additional specimens underwent precision additive dressing (PAD). The intention was to add SCC resistance precisely where it's necessary, while maintaining practical joint strength. A schematic of the PAD procedure is displayed in Figure 3. "Pass 1" was welded using "Filler Wire 1," and provides joint strength. Then, "Pass 2" was added using an inert "Filler Wire 2," and provides corrosion resistance to the FOZ of "Pass 1." Herein, "Filler Wire 1" is AA 5356 welded with the parameters described in prior work [6], and "Filler Wire 2" is AA 4043 welded with the low-dilution, cold metal transfer (CMT) process with a Fronius power supply; the wire-feed speed and travel speed were set to 4.6 m/min and 1.40 m/min, respectively. The area of the specimen covered by the CMT "Pass 2" may be referred to as the "dressed" region. It is noted that PAD can be conducted with differing filler wires, welding parameters, and welding equipment.

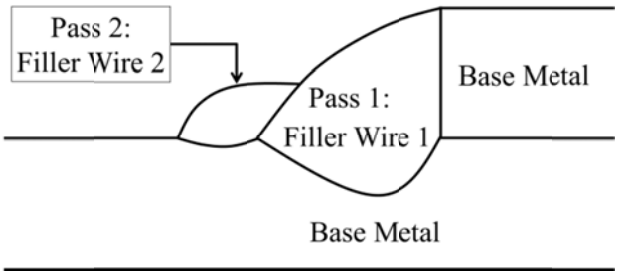

Figure 3: A schematic of the PAD procedure

For the purpose of SCC testing, the following specimen preparation was conducted, after all subsequent experimental changes were conducted to the initial, welded lap-joint. Figure 4 shows

a schematic of the specimen geometry. On the initial lap-joint, the 150 mm longitudinal weld length (along BM TD) was cut into four 25 mm sections. The length transverse to the weld (along BM RD) was cut to 150 mm, with the lower WT equidistant from both ends. The resulting specimen geometry is 150 x 25 x 8 mm, where both the top and bottom plates are nominally 4 mm thick.

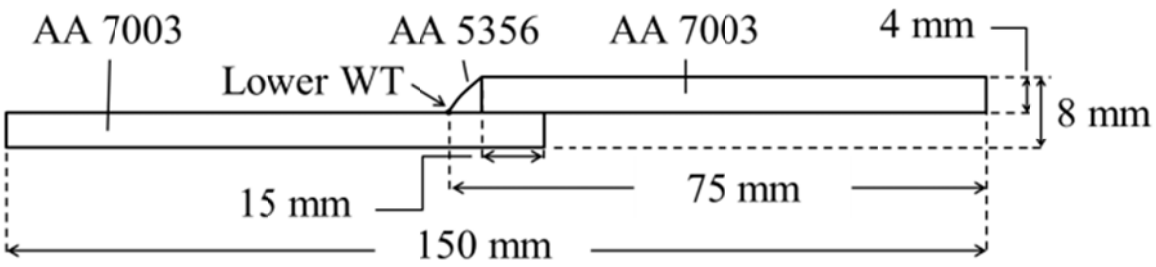

Figure 4: Schematic of a welded specimen (dimension into page: 25 mm).

The prepared specimen was inserted into a 3-point bend fixture, and displaced by 5 mm, generating tensile strain across the lower WT and in the HAZ. The statically stressed specimen was inserted into a cyclic corrosion test (CCT) chamber with a saline fog for SCC testing; details of the specimen loading (stressing) and SCC testing parameters are described within prior work [6].

To compare differences in the 2D surface-strains generated on the cross-section of SCC test specimens with differing geometry, a digital image correlation (DIC) study was conducted, prior to corrosion testing.

The specimens for DIC were polished, using 240, 320, 400, and 600-grit sand-paper, on one edge. Next, a flat-finish, white spray-paint was applied in a very thin coat to the polished specimen edge. After allowing at least 5 minutes for the white paint to dry, a flat-finish, black

spray-paint was applied from approximately 2 meters away; a very fine black & white speckle pattern resulted on the polished edge.

Initially, the speckled specimen was loaded into the SCC test 3-point bend fixture, with zero displacement. A dial caliper was placed in a manner to measure the vertical displacement of the lower WT (see Figure 4 for location of Lower WT). A camera, equipped with a macro lens, was placed on a tripod to capture incremental pictures as the specimen was displaced. In other words, starting at 0 mm lower WT displacement, a picture was taken of the specimen's speckle pattern every 0.25 mm of displacement until 5 mm total lower WT displacement was obtained.

To determine the 2D strain induced on the specimen's edge by the SCC testing fixture, the obtained pictures were chronologically ordered and input to the Ncorr software [34]. The key parameters for the Ncorr software are subset radius, subset spacing, strain radius, and subset truncation; these were set to 200 pixels, 15 pixels, 10 pixels, and "disabled," respectively. Because of high strains and a "crack-like" notch region, an exception was made with the EDM notched specimen; the subset truncation was "enabled."

Further corrosion testing was conducted in a more aggressive (than saline fog) environment, a heated chromic-acid solution. The specimen preparation and loading for such aggravated SCC testing is identical to that previously described.

The chromic-acid solution is mixed in a temperature- and acid-resistant, Pyrex container. Distilled water (1L of H_2O) is mixed with NaCl (3 g), CrO_3 (36 g), and $K_2Cr_2O_7$ (30 g). To fully dissolve the solute, the Pyrex container is placed on a hot plate with magnetic stirring capability. The temperature of the hot plate is set to increase the solution temperature to at least 75°C. As the water from the solution evaporates, additional distilled water is added to maintain the

solution concentration. Aluminum foil is placed atop the Pyrex container to minimize evaporation; this foil is removed every 15 minutes to visually inspect the specimen for cracking. The specimen is removed if a crack is noted, or if 16 hours of testing has elapsed. After the initial 8 hours of testing, the solution is allowed to cool and the specimen is removed from the environment; testing is paused until the next day when it resumes for an additional 8 hours.

3. Results and discussion

3.1. Digital Image Correlation

DIC has confirmed that geometric alterations to a test specimen do affect the strain state of a loaded specimen's cross-section. Figure 5 displays color-maps of horizontal micro-strain ($\mu\varepsilon_{xx}$) on each specimen's cross-section. The bounds of the color-bar (-4000 – 20000 με) are consistent for each specimen. Also, in Figure 5, the HAZ region that has shown the most pitting susceptibility (0 mm – 1 mm from FL; see Figure 7) is highlighted and labeled "Pitting". Note that the specimen's surface strain was created prior to corrosion exposure.

Within the region labeled "Pitting", the as-welded geometry had the lowest magnitude of strain (7000 με); the milled and EDM specimens had, respectively, 2x (15000 με) and 7x (50000 με) the magnitude of tensile strain within the same. However, using Equation 1 it was approximated that any strain beyond ~4000 με is plastic, thus each specimen possessed plastic strain in the HAZ.

Equation 1: An approximation of maximum elastic strain, beyond which plastic strain occurs.

$\varepsilon_y \approx \frac{\sigma_y}{E}$, where σ_y is the BM's yield stress, and E is Young's elastic modulus.

In addition to strain magnitude, Figure 5 shows that the strain was most concentrated in the EDM specimen. However, the tensile strain was also more concentrated in the milled specimen than the as-welded specimen. These results show that one main factor of SCC, (ii) stress intensity, was affected by the geometric alterations. However, neither geometric change reduced the magnitude of strain in the HAZ.

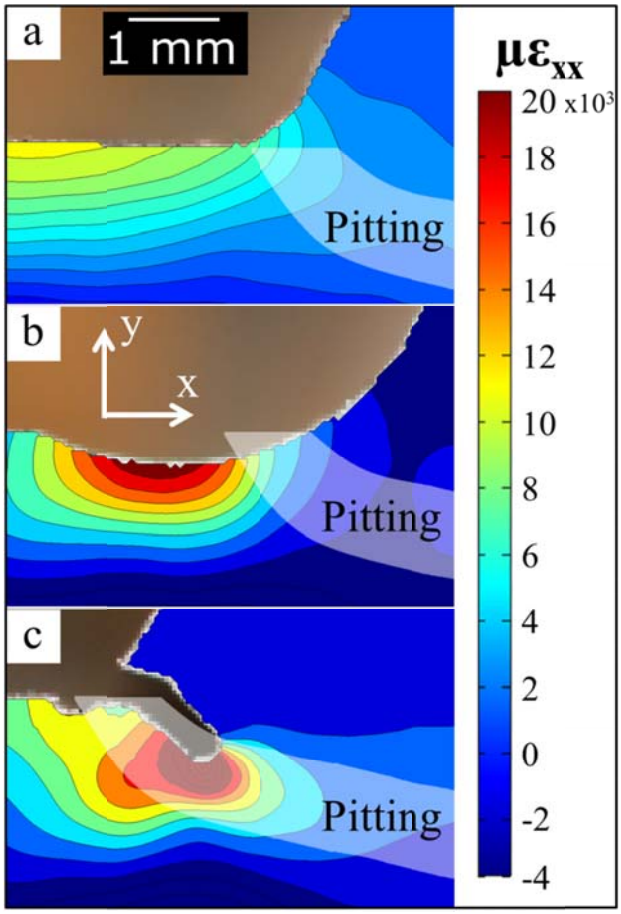

Figure 5: DIC results showing horizontal strain (ε_{xx}) and the location of maximum strain for, a) as-welded; b) milled; and c) EDM notched specimens

3.2. SCC Testing

Physically removing the FOZ by milling has eliminated SCC cracking within the milled test specimens (Figure 6). However, after a long time of exposure, the specimens showed preferential pitting in the HAZ between 0 mm and 1 mm from the fusion line; this is shown in Figure 7. The HAZ thermal cycle of as-welded and milled specimens was identical. However, milled specimens show less susceptibility to SCC. Noting that the DIC strain magnitude of milled specimens were 2x higher than as-welded specimens within the "Pitting" region, it's was determined that the HAZ precipitate morphology must contribute less to SCC initiation than the microstructure within the FOZ; this aligns with claims of prior studies [5] [6].

The following hypothesis explains why milled specimens were resistant to SCC, while as-welded were susceptible. In a cracked as-welded specimen, the dissolution of T phase within the FOZ led to local solution acidification within the formed pit [19]. The acidified FOZ pit interacts with the pitting-susceptible region of the HAZ directly below, and increases the pitting corrosion rate [20]. The accelerated pit growth led to a defect of critical size (imparting K_{ISCC}) that didn't occur in milled specimens.

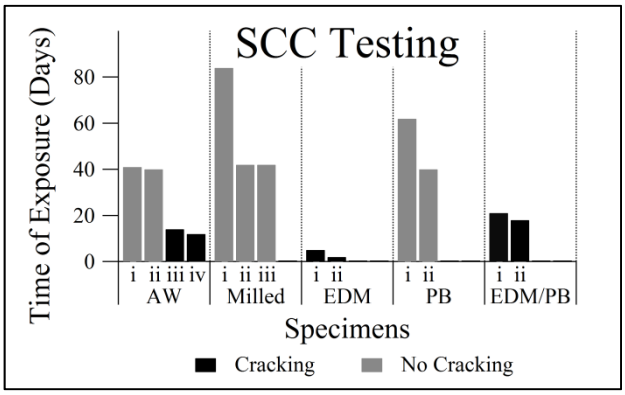

Figure 7: SCC test results showing specific specimen cracking response and time of exposure to the CCT environment

The results in Figure 6 show that each EDM specimen cracked with minimal time of exposure (*i.e.* 5 and 2 days). Comparatively, AW specimens iii and iv cracked after 14 and 12 days, respectively; this reveals that the incubation time for cracking is at least 2x less in EDM specimens. Incubation time is generally associated with the development of critical defects for SCC [26] [35]. It was noted that the difference in time-to-failure between EDM specimens i and ii may be related to the slightly different locations of the EDM notch with respect to the fusion line (Figure 8). Figure 8 shows that the EDM notch within specimen i (Figure 8c) is qualitatively farther from the FL than within specimen ii (Figure 8d).

Figure 6: Preferential pitting of the HAZ

The shorter incubation time for EDM specimens was attributed to stress intensity's proportionality to crack length $\left(K_I \propto \sqrt{a}\right)$. Physical evidence of strain localization was also shown in the DIC study (Figure 5).

The specimens that were exposed to a PB thermal cycle display resistance to SCC (Figure 6). No cracking is experienced in the two specimens tested at 5 mm displacement.

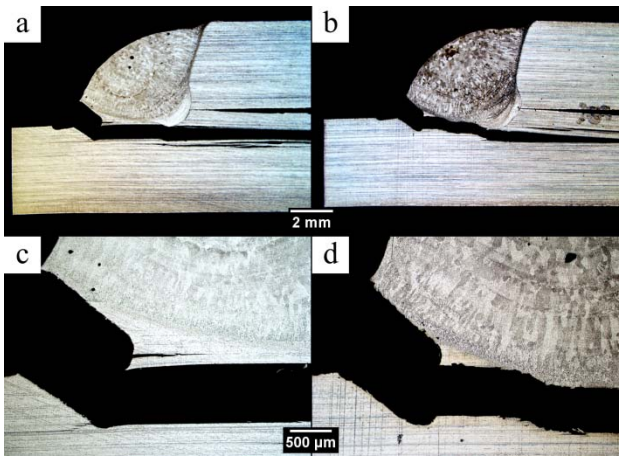

Figure 8: Two distinct EDM specimens that were SCC tested where: (a) and (b) are macrographs of specimens EDM_i and EDM_ii, respectively; (c) and (d) are micrographs of the same

To contrast the corrosion resistance of PB specimens, a specimen in the AW condition, that was displaced to 3 mm (no AW specimens cracked at this displacement [6]) and exposed to the SCC testing environment for 41 days, is paired with the PB specimen in Figure 9. The PB specimen in Figure 9 was exposed to the SCC testing environment for 62 days at 5 mm displacement; this is more time of exposure and induced specimen strain than the contrasting AW specimen within Figure 9.

The macrographs within Figure 9a-b show the similar geometry between the different test specimens. Thermodynamically, the post-weld, PB would cause coarsening of T precipitates within the PB specimen. It was noted that the distribution of FOZ T phase was inhomogeneous in the AW specimen, but homogeneous in the PB specimen (Figure 9c-d). It is hypothesized that the inherent inhomogeneity of FOZ T phase in AW specimens causes the inconsistency in SCC cracking response shown in Figure 6.

The un-etched micrographs (Figure 9e-f) highlight the difference in corrosion damage during SCC testing. The PB specimen exhibited extensive corrosion of the T precipitation network within the FOZ, but no corrosion damage penetrates the through-thickness of the BM HAZ. Conversely, the AW specimen exhibits pitting to a depth of 75 μm; the pitting initiates directly below FOZ corrosion damage. This evidence supports the hypothesis that corrosion of FOZ T phase directly accelerates HAZ pitting. It is speculated that the pitting in the AW specimen would have initiated SCC, had the specimen been displaced to a greater magnitude (i.e. 5 mm).

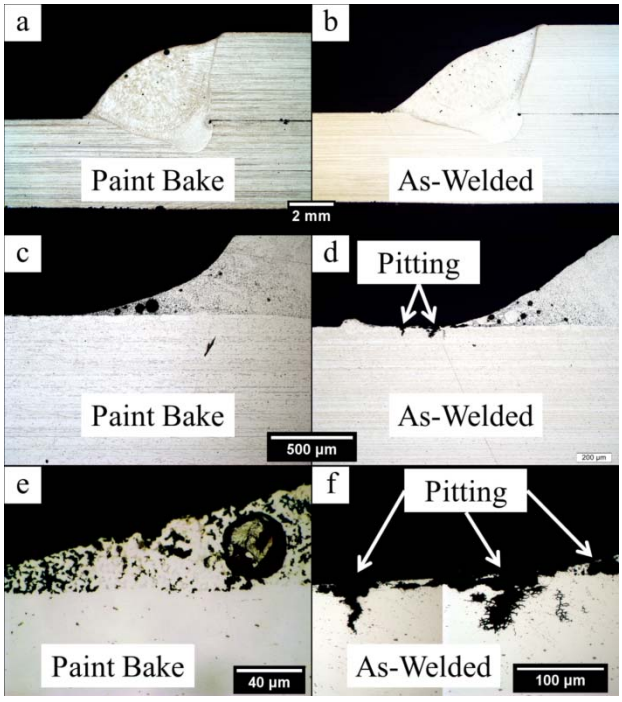

Figure 9: SCC tested specimens where: (a) and (b) are, respectively, macrographs of PB and AW specimens with a respective displacement/time of exposure of 5mm/62days and 3mm/41days; comparing corrosion damage, (c) and (d) are micrographs of the same; magnifying the differences in corrosion during testing, (e) and (f) are un-etched micrographs of the same

The metallographic evidence in Figure 9 supports the notion that a PB thermal cycle increases resistance to HAZ pitting. It's hypothesized that the similarity to the retrogression thermal cycle explains an increase in corrosion resistance.

The longer incubation times associated with EDM/PB specimens (Figure 6) compared to the EDM specimens support an increase in corrosion resistance due to the PB thermal cycle.

However, the cracking of EDM/PB specimens revealed that the PB thermal cycle does not cause resistance to SCC.

3.3. Aggravated SCC Testing

The time-to-failure data for each tested experimental condition is portrayed within Figure 10. Of the AW specimens, 60% exhibited cracking (iii, iv, & v) before 3 hours of test exposure, while the other specimens (i & ii) showed more resistance to cracking. Such resistance to cracking is speculated to be related to the random, inhomogeneous FOZ T phase distribution identified in Figure 9d. Contrasting the standard SCC testing results, both PB specimens exhibited cracking before 3 hours. Also, a milled specimen showed cracking before 3 hours. The PAD specimen exhibited cracking after 5.5 hours, but the crack did not occur in the dressed region.

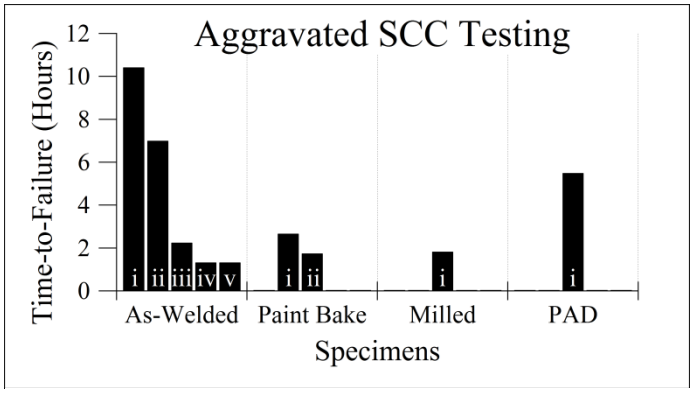

Figure 10: Time-to-failure results of aggravated SCC testing for specific experimental conditions, where specific specimens are labeled i-v.

The results of the acid corrosion testing showed that every experimental condition is susceptible to corrosion by chromic acid, but there was variability in the path of cracking between experimental conditions. Figure 11 a-b shows that failures in the AW conditions initiate within the FOZ but penetrate 50-200 μm into the BM (HAZ) before connecting with the FL via an anisotropic grain boundary within the BM. However, specimens exposed to the PB thermal cycle didn't exhibit cracks that penetrate into the BM, but instead initiated within the FOZ, and exclusively followed the FL; the inflection noted in crack propagation within Figure 11 c-d is

notably different from that experienced in Figure 11 a-b. In other words, if the cracking noted within Figure 11a is described as concave, the cracking in Figure 11b would be described as convex. This difference was consistent with additional specimens of like

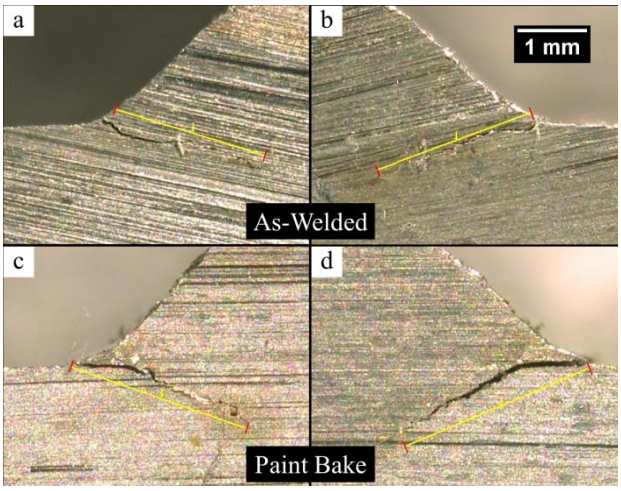

Figure 11: Micrographs of acid test specimens where: (a) edge A and (b) edge B of an as-welded specimen; (c) edge A and (d) edge B of a paint bake specimen

experimental condition, and provides further evidence for superior corrosion resistance in the HAZ of specimens that experienced a PB. However, this experiment showed that in more acidic environments, the PB did not prevent cracking.

Showing the stress-dependence of cracking, an AW specimen, tested with 0 mm displacement in the aggravated SCC test, exhibited no cracking along the fusion line after 16 hours of exposure. However, severe pitting was noted in the lower HAZ to a distance of 1 mm beyond the fusion line.

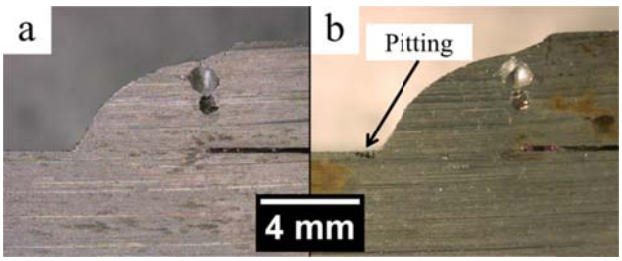

Figure 12: AW test specimen displaced to 0 mm in the aggravated SCC environment, where a) Specimen edge before test exposure; b) Specimen edge after test exposure

The milled and PAD test specimens are displayed in Figure 10. In addition to the cracking noted in the typical location (lower HAZ), extensive corrosion damage was noted in the HAZ (short transverse direction), just beyond the upper weld toe. In environments more acidic than salt water, milled specimens were also susceptible to catastrophic cracking.

The PAD specimen (Figure 10b) exhibited corrosion resistance in the dressed region. After 5.5 hours of test exposure, cracking occurred in the un-dressed, upper weld toe. The AW specimens that experienced more than 3 hours of test exposure (i and ii) also exhibited cracking in the upper weld toe. The lack of cracking in the dressed, lower weld toe of the PAD specimen, due to the precisely added AA 4043, underlines the increase in corrosion resistance due to PAD.

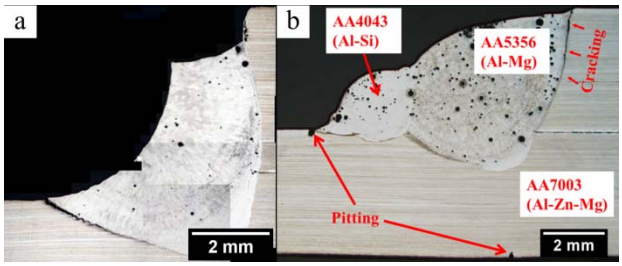

Figure 13: Macrographs of acid tested specimens, where a) milled; b) PAD

Lap-shear tensile testing was conducted on a PAD specimen; results showed consistent properties with AW specimens. The yield stress was 120 MPa and the ultimate tensile stress was 263 MPa. Previous studies [6] [33] showed that other SCC mitigation techniques (*i.e.* AA 4043 filler wire, milling, and friction stir processing) each decreased the joint strength.

Being nothing more than a 2nd weld pass, albeit a low-dilution (*e.g.* CMT) weld pass, PAD proved to be a practical process for SCC mitigation that is applicable to complex geometries, and suitable for high production.

4. Theory for accelerated SCC in AA GMAW

GMAW of AAs leads to a FOZ that covers approximately 1 mm of the HAZ. The HAZ is susceptible to preferential pitting corrosion from a distance 0 to 1 mm beyond the fusion line. The FOZ contains a secondary phase (intermetallic) that, if anodic to the aluminum matrix, experiences preferential pitting. The pits, occurring within the FOZ, generate a more acidic (lower pH) local environment [19]; the acidified environment interacts with the pitting-

susceptible HAZ immediately below the FOZ. Accelerated growth of corrosion damage subsequently occurs in the HAZ (Figure 9f) [20]. Upon the development of a critical defect, the geometry and environment within the HAZ defect, combined with an external tensile load, generates SCC within the exposed short transverse direction of the HAZ. Each of the necessary factors for SCC (*i.e.* corrosive environment, tensile stress, and susceptible material) is affected by arc-welding. In a saline solution, the corrosive environment becomes more acidic because of FOZ pitting; tensile stress intensity is increased because of FOZ and HAZ corrosion damage; the material's susceptibility to SCC in the HAZ is increased because of the weld thermal cycle. Catastrophic SCC is experienced in an accelerated timeframe due to arc welding. Solid-state welds do not generate a FOZ, and are, therefore, less susceptible to SCC.

5. Conclusions

- Physically milling away the FOZ decreased the SCC susceptibility of the welded joint.
- Increasing the stress intensity within the HAZ with an EDM notch increased the joint's SCC susceptibility, causing the specimens to fail at least two times faster.
- Exposing a specimen to a PB thermal cycle decreased the joint's HAZ pitting susceptibility, which led to decreased SCC susceptibility. PB specimens did not crack, while EDM/PB specimens experienced an increased incubation time prior to cracking.
- Every joint condition showed susceptibility to cracking during aggravated testing (chromic acid). However, the "dressed" region of the PAD specimen exhibited excellent cracking resistance.

References

[1] M.G. Mousavi, C.E. Cross, O. Grong, and M Hval, *Sci. Technol. Weld. Join.*, vol. 2, pp. 275-278, 1997.

[2] S. Yang and Q. Lin, *Adv. Mater. Res.*, vol. 148-149, pp. 640-643, 2011.

[3] S Kou, *Welding Metallurgy*, 2nd ed. New York: Wiley, 2003.

[4] C.M. Liao, *Corrosion*, vol. 49, no. 1, pp. 52-59, January 1993.

[5] T.E. Borchers, D.P. McAllister, and W. Zhang, *Metall. Mater. Trans. A*, vol. 46A, pp. 1827-1823, 2015.

[6] T.E. Borchers, A. Seid, S.S. Babu, P. Shafer, and W. Zhang, *Sci. Technol. Weld. Join.*, vol. 20, pp. 460-467, 2015.

[7] M.C. Reboul, B. Dubost, and M. Lashermes, *Corrosion Science*, vol. 25, pp. 999-1018, 1983.

[8] A. K. Jha, G. N. Shiresha, and K. Sreekumar, *Engineering Failure Analysis*, vol. 15, pp. 787-795, 2008.

[9] G.S. Frankel and Z. Xia, *Corrosion*, vol. 55, no. 2, pp. 139-150, 1999.

[10] M.O. Speidel, *Met. Trans.*, vol. 6A, p. 1975, April 1975.

[11] N.J.H. Holroyd, A.K. Vasudevan, and L. Christodoulou, *Treatise on Materials Science and Technology*, vol. 31, p. 463, 1989.

[12] M. Baumgartner and H. Kaesche, *Corrosion*, vol. 44, no. 4, pp. 231-239, April 1988.

[13] D.O. Sprowls and R.H. Brown, *Fundamental Aspects of Stress Corrosion Cracking*, R.W. Staehle, Ed. Houston, United States: National Association of Corrosion Engineers, 1969.

[14] R. Braun, *Mat.-wiss. u. Werkstofftech*, vol. 38, no. 9, pp. 674-688, 2007.

[15] T.D. Burleigh, *Corrosion*, vol. 47, no. 2, pp. 89-97, 1991.

[16] G. Lu and et al., "Hydrogen Enhanced Local Plasticity in Aluminum: An Ab Initio Study," Harvard University, 2002.

[17] S.P. Lynch, *Acta Metall.*, vol. 36, p. 2639, 1988.

[18] D. Najjar, T. Magnin, and T.J. Warner, *Mater. Sci. Eng., A*, vol. 238, pp. 293-302, 1997.

[19] J.R. Galvele, *Corros. Sci.*, vol. 21, no. 8, pp. 551-579, 1981.

[20] B. Zaid, D. Saidi, A. Benzaid, and S. Hadji, *Corros. Sci.*, vol. 50, pp. 1841-1847, 2008.

[21] M. Nicolas and A. Deschamps, *Acta Mater.*, vol. 51, pp. 6077-6094, 2003.

[22] I.L. Muller and J.R. Galvele, *Corros. Sci.*, vol. 17, pp. 995 - 1007, 1976.

[23] J. Dabrowski and J.R. Kish, *Corros.*, vol. 71, pp. 895-907, 2015.

[24] Y. Deng et al., *Corros. Sci.*, vol. 100, pp. 57-72, 2015.

[25] M. Nicolas and A. Deschamps, *Metall. Mater. Trans. A*, vol. 35A, pp. 1437-1448, May 2004.

[26] N.J.H. Holroyd and G.M. Scamans, *Metall. Mater. Trans. A*, vol. 44A, pp. 1230-1253, 2013.

[27] Y.E. Wu and Y.T. Wang, *Theor. Appl. Fract. Mech.*, vol. 54, pp. 19-26, 2010.

[28] M. Baydogan, H. Cimenoglu, S Kayali, and J. Rasty, *Metall. Mater. Trans. A*, vol. 39A, pp. 2470-2476, 2008.

[29] A. Zelinski, J. Chryzanowski, M. Warmuzek, A. Gazda, and E. Jezierska, *Mater. Corros.*, vol. 55, no. 2, pp. 77-87, 2004.

[30] A. Thakur, R. Raman, and S.N. Malhotra, *Mater. Chem. Phys.*, vol. 101, pp. 441-447, 2007.

[31] R.Y. Hwang and C.P. Chou, *Scripta Materialia*, vol. 38, no. 2, pp. 215-221, 1997.

[32] G.M. Ugiansky, L.P. Skolnick, and S.W. Steifel, *Corrosion*, vol. 25, pp. 77-86, 1969.

[33] T.E. Borchers et al., "Stress Corrosion Cracking Susceptibility of Gas Metal Arc Welded 7xxx Series Aluminum Alloys," in *Sheet Metal Welding Conference XVI*, Detriot, 2014.

[34] J. Blaber, B. Adair, and A. Antoniou, *Exp. Mech.*, vol. 55, pp. 1105-1122, 2015.

[35] K.R. Cooper and R.G. Kelly, *Corros. Sci.*, vol. 49, pp. 2636-2662, 2007.

[36] P.K. Rout, M.M. Ghosh, and K.S. Ghosh, *Mater. Sci. Eng. A*, vol. 604, pp. 156-165, 2014.

[37] P.B. Srinivasan, W. Dietzel, R. Zettler, J.F. dos Santos, and V. Sivan, *Mater. Sci. Eng. A*, vol. 392, pp. 292-300, 2005.